J. Radiat. Res., 53, 272–280 (2012)

A Treatment Planning Comparison of Passive-Scattering and Intensity-Modulated Proton Therapy for Typical Tumor Sites

Yuki KASE[1,2]*, Haruo YAMASHITA[1,2], Hiroshi FUJI[2], Yuichi YAMAMOTO[3], Yuehu PU[3], Chihiro TSUKISHIMA[3] and Shigeyuki MURAYAMA[1,2]

IMPT/Proton therapy/Beam scanning/Treatment planning.

Intensity-modulated proton therapy (IMPT) is expected to improve treatment results with fewer side effects than other proton therapies. The purpose of this study was to evaluate the tumor sites for which IMPT was effective under the same beam calculation conditions by planning IMPT for typical cases treated with passive scattering proton therapy (PSPT). We selected 16 cases of nasal cavity, lung, liver or prostate cancers as typical tumor sites receiving PSPT. The dose distributions and dose volume histograms optimized by the IMPT were compared with those optimized by the PSPT. We took particular note of the doses to the skin and organs at risk (OAR) when PSPT was replaced by IMPT. Furthermore, an improvement of the beam angles was also performed to obtain better dose distributions in the IMPT. The IMPT with the same beam angles resulted in near-maximum doses to the skin of average 78%, 64%, 84% and 99% of the PSPT doses for nasal cavity, lung, liver, and prostate cancers, respectively. However, it was difficult to improve the dose homogeneity of the target volume. The change of the IMPT beam angles could reduce the doses to OARs and skin in the case of the nasal cavity, while it had limited effect in the other cases. We concluded that IMPT was effective for reducing the doses to some OARs when treating nasal cavity, lung, liver and prostate cancers. The selection of beam angles was important in the IMPT optimization, especially for nasal cavity cancers.

INTRODUCTION

Proton beams can concentrate the absorbed dose to a target volume deeply seated in a patient's body better than conventional photon beams by means of their excellent dose distribution, known as the Bragg peak.[1)] Proton therapy was started at the Lawrence Berkeley National Laboratory in the United States in 1954, and it has been performed as part of modern radiotherapy at about 30 facilities in many countries.[2)] Moreover, new proton treatment projects have been proposed around the world.

In proton therapy, there are mainly two irradiation approaches to forming therapeutic beams for cancer treatment. One method is the passive scattering technique, in which the beam-scattering material, range modulator, range shifter and collimator are used to form the treatment beam that spreads out to the target volume.[3,4)] Passive scattering proton therapy (PSPT) was developed for early patient treatment and commonly implemented in most of the proton treatment facilities. Another method is the active scanning technique, in which scanning magnets are used to scan a narrow pencil beam in three dimensions through the target volume.[5,6)] Scanning particle beam therapy can reduce unnecessary doses to normal tissues around the target volume so that secondary cancer risk can be expected to be reduced in and out of the radiation field.[7)] The active scanning technique made it possible to perform intensity-modulated proton therapy (IMPT). IMPT has already been performed through the development of the fast beam scanning technique and the dose optimization algorithm at Paul Scherrer Institute in Switzerland.[8–10)] Many authors have reported the dose distribution calculated for IMPT.[11,12)]

At Shizuoka Cancer Center (SCC), proton therapy has been implemented using a medical proton synchrotron since 2003.[13)] As of this writing, more than 1,000 patients with

*Corresponding author: Phone: +81-55-989-5222,
Fax: +81-55-989-5634,
E-mail: y.kase@scchr.jp

[1]Proton Therapy Division, Shizuoka Cancer Center Research Institute, 1007, Shimonagakubo, Nagaizumi, Shizuoka 411-8777, Japan; [2]Proton Therapy Division, Shizuoka Cancer Center Hospital, 1007, Shimonagakubo, Nagaizumi, Shizuoka 411-8777, Japan; [3]Energy System Center, Mitsubishi Electric Corporation, 1-1-2, Wadasaki, Hyogo, Kobe 652-8555, Japan.

doi:10.1269/jrr.11136

various tumors including head and neck, lung, liver and prostate cancers have been treated by PSPT with the rotating gantry at SCC. The beam scanning irradiation technique has been under study as a way to achieve more effective proton therapy as a next-generation treatment. The purpose of this study is to evaluate which cases will be effectively improved by the use of IMPT as compared with PSPT in terms of the proton dose distribution. In this study, treatment planning of the IMPT was performed for typical treatment cases. The beam angle dependence of the dose distribution achieved by the IMPT was also investigated to determine the additional advantage of the IMPT. This study will yield information of value to the development of an efficient beam scanning system.

MATERIALS AND METHODS

Patient selection for comparison of IMPT and PSPT

We selected 16 cases of nasal cavity, lung, liver or prostate cancer as typical tumor sites treated with PSPT. Therapeutic aim and possible side effects were thoroughly discussed with patients and informed consent was obtained before treatment. Table 1 lists the treatment conditions of the cases selected for the proton therapy. The generally accepted RBE value of 1.1 for therapeutic proton beam was used to give the RBE-weighted absorbed dose.[2)] For instance, 1.0 Gy in proton absorbed dose equals to 1.1 Gy(RBE) in RBE-weighted absorbed dose. Boost irradiations of the prostate cancers were not considered in this study because the planning target volume (PTV) of the boost plan was different from the PTV of the initial plan, and the dose distributions were separately evaluated against each PTV.

Table 1. Therapeutic conditions for the PSPT selected for this study.

Case	Tumor site	PTV (cm^3)	Dose (Gy(RBE))	# of fractions	# of beams
1	Ethmoid sinus	81	70.0	28	3
2	Orbital cavity	32	70.0	28	3
3	Ethmoid sinus	30	60.0	24	6
4	Maxillary sinus	267	65.0	26	2
5	Upper lung	64	80.0	20	3
6	Upper lung	13	65.0	10	2
7	Middle lung	67	72.0	30	3
8	Upper lung	134	66.0	33	2
9	Liver (S4)	83	63.0	10	3
10	Liver (S6)	28	64.8	10	3
11	Liver (S8)	168	39.2	14	2
12	Liver(S7,S8)	117	76.0	20	3
13	Prostate	93	50.0	25	2
14	Prostate	160	50.0	25	2
15	Prostate	100	50.0	25	2
16	Prostate	104	50.0	25	2

The computed tomography (CT) images of the selected patients were taken for the PSPT with a slice spacing of 2 mm over the entire treatment area with sufficient margins in both superior and inferior directions. Target volumes and organs at risk (OAR) were delineated on the CT images by radiation oncologists. Then, the CT slices used for the treatment planning were decided to include entire PTV and more than 10 cm scan regions (50 slices) extended beyond the PTV in both superior and inferior directions. These patients were retrospectively re-planned using IMPT with the same CT images, target volumes and OARs.

The chiasm, optical nerves, and eyes around the target were used as the typical OARs in nasal cavity cancer. The spinal cord and normal lung, defined as the one-lung volume after the removal of the gross tumor volume (GTV), were used as the OARs in lung cancer cases. The normal liver, defined as the liver volume after the removal of the GTV, was used as the OAR in liver cancer cases. The rectum and bladder were used as the OARs in prostate cancer cases. For the IMPT optimization, partial skin volume was treated as an additional OAR by the contouring of a 5 mm thickness from the body surface on CT slices near the PTV.

The three-dimensional setup margin for the PTV was set at 3 or 5 mm from the clinical target volume (CTV) in nasal cavity cancer. The setup margin of 5 mm from the internal target volume (ITV) was used in lung and liver cancer. The ITV was defined as the CTV plus an internal margin due to a respiratory displacement for each patient. The internal margin was decided from 5 to 8 mm in moving direction in consideration with the CT images taken during both inspiration and expiration. The setup margin of 5 mm from the CTV was used in prostate cancer. The contours of the PTV were then fine-tuned by the radiation oncologist or physicist as appropriate. Each reference point for dose prescription was put at the center of the GTV.

Treatment planning system for PSPT

The proton treatment facility at SCC has consisted of the ion source, radio frequency quadrupole linear accelerator, 235 MeV synchrotron, high-energy beam transport, one horizontal irradiation room and two gantry irradiation rooms made by Mitsubishi Electric Corporation. Proton kinetic energies of 150, 190, and 220 MeV have been regularly used for PSPT in clinical practice. The beam delivery system has included beam-wobbling magnets, a lead scatterer, ridge filter, beam monitors, range shifter, and beam collimator to form proton treatment beams. The ridge filters were installed downstream of the scatterer to make spread-out Bragg peaks ranging in length from 30 to 120 mm in increments of 10 mm.[14)] The dose calculation was performed with a pencil-

beam algorithm using the treatment planning system named XiO-M (ELEKTA CMS software), which was extended for the PSPT by the Mitsubishi Electric Corporation.[15–17] The stopping power ratio was approximated using the effective density measured by planning X-ray CT with appropriate CT number conversion.[18]

Beam parameters for the IMPT

We assumed the use of spot-scanning proton beams when mounting beam scanning magnets and the fast range shifter in the rotating gantry room in the proton facility at SCC. Range modulation for the scanning pencil beam was supposed to be controlled by both the extraction energy from the synchrotron and the range shifter thickness. XiO software for planning spot scanning for proton therapy (ELEKTA) was used to optimize the treatment dose distribution for the IMPT on the CT images. Physical input parameters of depth-dose distributions and beam spot sizes for the spot-scanning proton beams were calculated by a Monte Carlo simulation in consideration of the irradiation geometry.

The Monte Carlo code GEANT 3.21.14 was used to calculate depth-dose distributions and spot sizes for the scanning beams, since it was flexible enough to make a set of subroutines to define the materials, geometries and particle properties.[19] Nuclear interactions between the protons and materials, the transport of secondary particles, and the multiple scattering and ionization loss of the charged particles were calculated in the GEANT program. The distance from the isocenter to the central position of the scanning magnets was set to be 2900 mm, and the distance from the isocenter to the central position of the range shifter was 670 mm. The water target on the isocenter was divided into voxels of a 1-mm cube to calculate the fundamental three-dimensional dose distributions for the scanning proton beams of the initial kinetic energies of 70, 115, 150, 190 and 220 MeV.

Figure 1 shows the depth-dose distributions of the scanning proton beams calculated by the GEANT program. The depth-dose distributions of the 150 and 190 MeV proton pencil beams were measured by the ionization chamber in the water column to confirm the calculated results. In least square fitting of a Gaussian function to the lateral dose profile in air at the isocenter, beam spot size was defined as the standard deviation of the Gaussian distribution. Figure 2 shows the beam spot size as a function of the range shifter thickness with respect to each initial beam energy. The calculated depth-dose distributions and spot sizes were entered into the XiO software to plan the spot scanning for proton therapy. Both depth-dose distribution and beam spot size calculated by GEANT 3.21 for scanned proton beams had been experimentally verified by Kimstrand *et al.*[20]

Optimization calculation of the IMPT

The XiO software has been able to optimize the dose distribution or dose volume histograms (DVH) of target volumes and OARs by the iterative calculation method. The same beam number and prescribed dose were applied in the treatment planning of both the IMPT and PSPT. The dose administered to the PTV that was received by 95% volume, D_{95}, was adjusted to 95% of the prescribed dose in the DVH. It was attempted to keep the dose administered to the PTV that was received by 5% volume, D_5, was tried to be smaller than 105% of the prescribed dose in the DVH. The maxi-

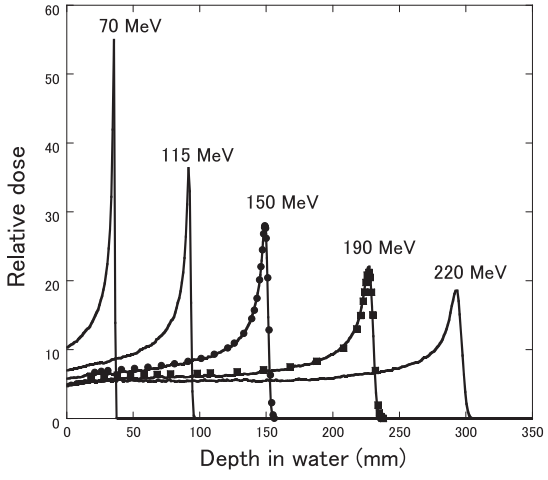

Fig. 1. Depth-dose distributions of the pristine proton beams used for the IMPT calculation. Lines show the GEANT calculation, which was input into the XiO software to plan the spot scanning for the proton therapy. Plots represent the ionization chamber measurement in the water column for the pencil-like proton beams with kinetic energies of 150 and 190 MeV.

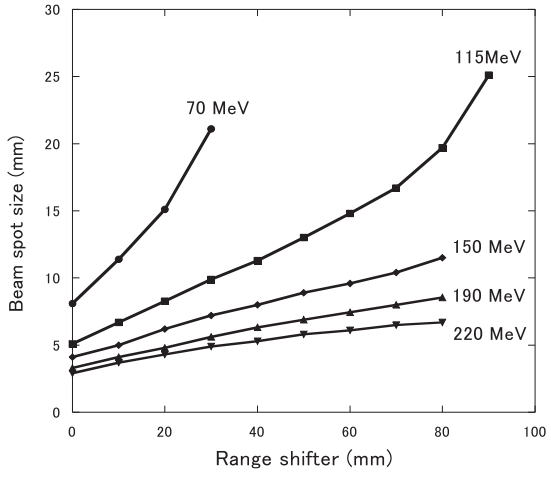

Fig. 2. Calculated beam spot sizes as a function of the range shifter thickness for each proton beam energy. The beam spot size means the standard deviation in least square fitting of a Gaussian function to the lateral dose profile in air at the isocenter. These results were input into the XiO software to plan the spot scanning for the proton therapy.

mum dose to each OAR for the IMPT optimization was set so that the tolerance dose for the occurrence of side effects would be 5% within 5 years after the treatment, $TD_{5/5}$, as reported by Emami *et al*.[21] In addition, the dose received by 20% volume, D_{20}, of each OAR was also set to half of the $TD_{5/5}$ value for the IMPT optimization. The scanning beam ranges were modulated by the selection of both accelerated beam energy and range shifter thickness for the respective beam spots.

The beam spot spacing between Bragg peaks was set at 7.5 mm orthogonal to the beam direction and 5 mm in depth. A peak width multiplier of 1.25 and a maximum iteration number of 100 were used for the IMPT optimization. Then, the optimized dose distribution and dose volume histograms (DVH) of the IMPT were compared with those of the PSPT for each case to estimate the suppression of side effects.

The beam angle dependence of the DVH for the IMPT calculation was also discussed to improve the dose distribution. The beam angles were changed in steps of 5 degrees to estimate the optimal combination of beam angles with the same beam numbers as the PSPT. We made a judgment as to whether the combination of the beam angles was optimum by checking the calculated DVHs to the OARs and skin in a comprehensive manner.

RESULTS

Cross-sectional dose distributions

Figure 3 shows visual comparisons of the dose distributions among the PSPT, the IMPT with same beam angles

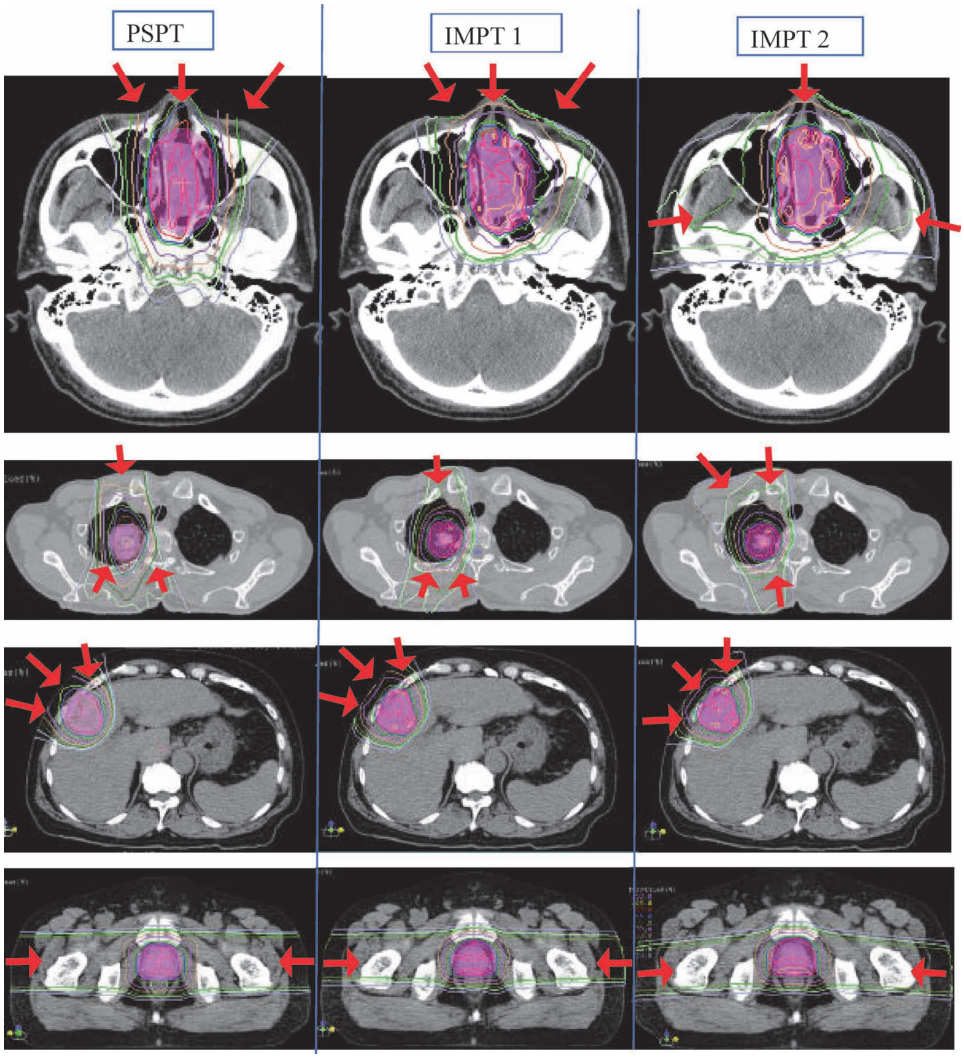

Fig. 3. Visual comparisons between the proton dose distributions calculated using the PSPT method and IMPT method in the treatment plans for nasal cavity (Case 1), lung (Case 5), liver (Case 9) and prostate (Case 13) cancers. Magenta areas represent the PTVs. Isodose levels show 105% (yellow), 100% (red), 95% (blue), 90% (green), 70% (purple), 50% (orange), 30% (dark green), 20% (light green) and 10% (light blue) of the reference point doses. Red arrows show the therapeutic beam directions.

(IMPT 1) and the IMPT with improved beam angles (IMPT 2) on cross-sectional CT images at the reference points in the treatment plans for typical nasal cavity, lung, liver and prostate cancers. The IMPT could improve the dose concentration, as shown, by around the 50% isodose line.

Figure 4 shows the off-center ratios calculated against the x-axis and y-axis on the reference point by the PSPT and IMPT in typical cases of nasal cavity cancer (Case 1) and prostate cancer (Case 13). Different dose distributions were observed near the inner boundaries of the PTV and penumbra regions in the PSPT and IMPT plans.

DVHs of the PTV and the OARs

Figure 5 shows the DVHs of the PTV and some OARs between the PSPT and the IMPT with the same beam angles in the treatment planning of the typical cancers of the nasal cavity (Case 1), lung (Case 5), liver (Case 9) and prostate (Case 13).

The doses received by 98% volume, D_{98}, and the doses received by 2% volume, D_2, of the PTV were used to indicate the 'near-minimum dose' and 'near-maximum dose', respectively, because artifacts in the calculation or display process can yield misleading lowest or highest doses.[2)] Table 2 indicates the near-minimum doses, D_{98}, and the near-maximum doses, D_2, of the PTV in the PSPT and IMPT calculations.

The dose homogeneities of the PTV with the D_{98} and D_2 values for the PSPT were about 95–104% for nasal cavity cancers, 95–103% for lung cancers, 95–102% for liver cancers, and 94–102% for prostate cancers. Thus, the dose homogeneity of the PTV was almost held within the ICRU limits of 95% to 107% of the prescribed dose for the tumor sites. However, it was difficult to improve the PTV dose homogeneity within the ICRU limits with IMPT despite the best efforts at IMPT optimization. In the IMPT, the homogeneities were 93–117% for the nasal cavity, 93–105% for the upper lobe of the lung, 92–105% for the right lobe of the liver, and 88–106% for the prostate. There was little difference in the dose homogeneities among the different beam angles selected in IMPT.

It was confirmed that IMPT could reduce the large doses to the OARs in nasal cavity, lung and prostate cancers.

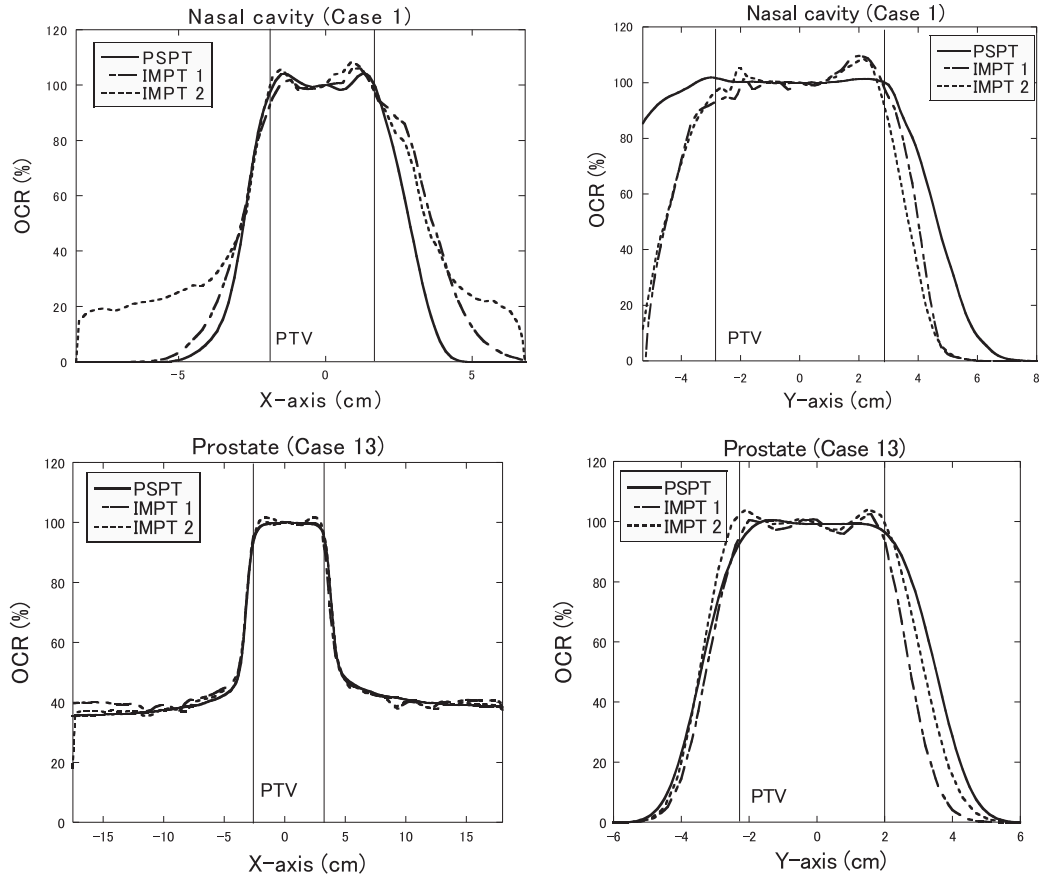

Fig. 4. Off-center ratios against the x-axis and y-axis on the reference point in the nasal cavity (Case 1) and prostate (Case 13) cancers. Solid, dashed and dotted lines indicate the PSPT, the IMPT with the same beam angles (IMPT 1), and the IMPT with improved beam angles (IMPT 2), respectively. The regions between the solid straight lines represent the PTV.

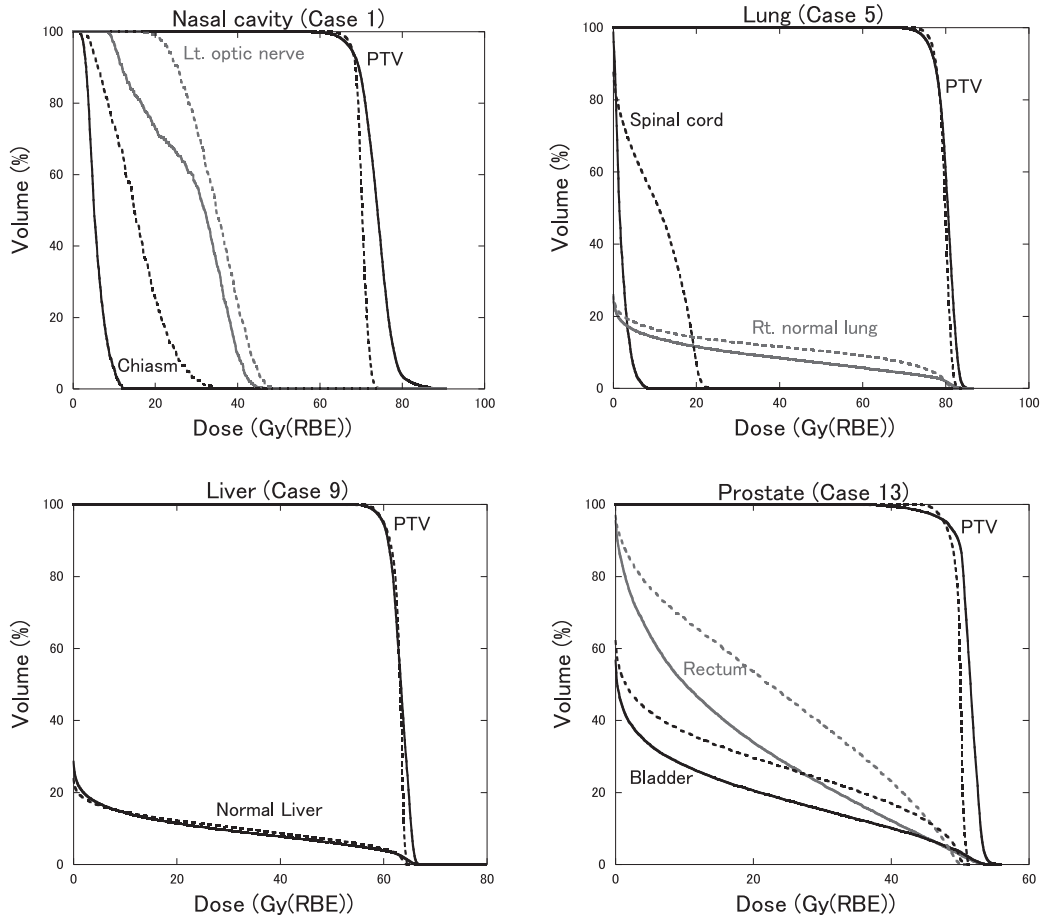

Fig. 5. Comparisons of dose volume histograms between IMPT (solid lines) and PSPT (dashed lines) with the same beam angles in the treatment planning for nasal cavity (Case 1), lung (Case 5), liver (Case 9) and prostate (Case 13) cancers.

Table 2. The near-minimum doses (D_{98}), near-maximum doses (D_2) and mean doses (D_{mean}) of the PTV in terms of Gy(RBE).

Case, site	Parameter	PSPT	IMPT 1	IMPT 2
Case 1, Ethmoid sinus	D_{98}	66.6	65.3	66.0
	D_2	73.0	82.0	79.4
	D_{mean}	70.4	73.2	73.1
Case 5, Upper lung	D_{98}	75.5	74.2	74.0
	D_2	82.0	83.7	86.3
	D_{mean}	79.7	80.9	80.2
Case 9, Liver (S4)	D_{98}	58.8	58.4	58.6
	D_2	64.4	66.0	66.1
	D_{mean}	62.9	63.3	63.3
Case 13, Prostate	D_{98}	46.7	44.2	44.8
	D_2	51.0	53.2	53.5
	D_{mean}	49.4	50.8	50.9

Meanwhile, IMPT could increase the doses to some OARs if the doses were less than the prescribed tolerance doses. For example, the near-maximum doses (D_2), doses received by 20% volume (D_{20}) and mean doses (D_{mean}) to OARs in Case 1 involving nasal cavity cancer are described in Table 3. The doses to the chiasm, left optic nerve and skin were obviously reduced by the IMPT, while those to the right optic nerve and eyes were conversely increased within the tolerance doses. The other cases showed similar tendencies for IMPT optimization. Table 4 summarizes the near-maximum doses to the skin calculated in the PSPT and IMPT plans for all cases in this study. It was found that the doses to the skin were almost reduced by the IMPT optimization. IMPT was effective to decrease the maximum dose to the skin in nasal cavity, lung and liver cancers, while it was not very effective in prostate cancer.

In nasal cavity cancers, the near-maximum doses to the skin were decreased to an average of 78% (range: 61–98%) of the PSPT doses by the IMPT with the same beam angles. The average D_{20} values administered to the chiasm, optical

Table 3. The near-maximum doses (D_2), doses received by 20% volume (D_{20}) and mean doses (D_{mean}) to the OARs in terms of Gy(RBE) for Case 1 involving nasal cavity cancer.

OAR	Parameter	PSPT	IMPT 1	IMPT 2
Chiasm	D_2	30.4	11.2	13.5
	D_{20}	21.3	7.3	8.6
	D_{mean}	15.3	6.3	6.2
Left optic nerve	D_2	46.6	43.2	42.4
	D_{20}	41.0	37.8	37.7
	D_{mean}	34.7	30.5	29.1
Right optic nerve	D_2	34.3	28.5	34.6
	D_{20}	27.8	21.1	26.3
	D_{mean}	15.6	17.0	19.0
Left eye	D_2	36.0	36.0	32.6
	D_{20}	21.0	23.0	21.1
	D_{mean}	15.2	18.0	14.7
Right eye	D_2	20.3	27.0	22.6
	D_{20}	11.2	16.3	14.3
	D_{mean}	4.8	12.1	10.2
Skin	D_2	54.9	38.1	33.7
	D_{20}	0.3	2.2	8.4
	D_{mean}	4.4	3.8	5.0

Table 4. The near-maximum dose to the skin for each irradiation method in terms of Gy(RBE).

Case	Tumor site	PSPT	IMPT 1	IMPT 2
1	Ethmoid sinus	55	38	34
2	Orbital cavity	65	54	52
3	Ethmoid sinus	59	58	58
4	Maxillary sinus	62	38	38
5	Upper lung	38	23	21
6	Upper lung	24	17	14
7	Middle lung	35	22	16
8	Upper lung	42	26	24
9	Liver (S4)	57	41	41
10	Liver (S6)	18	16	17
11	Liver (S8)	39	31	31
12	Liver(S7,S8)	55	52	51
13	Prostate	18	20	20
14	Prostate	20	21	21
15	Prostate	19	16	18
16	Prostate	20	19	19

nerve and eyes were 38% (2–76%), 94% (77–125%) and 87% (32–132%) of the PSPT, respectively. The cases involving increases of more than 100% were of slight importance since the doses were much lower than the tolerance doses. Therefore, the use of IMPT was able to decrease the relatively large doses to the OARs in the case of the nasal cavity.

In lung cancer, the near-maximum doses to the skin were decreased to an average of 64% (61–71%) of the PSPT doses by the IMPT with the same beam angles. The D_{20} values of normal lung of the tumor side and spinal cord averaged 46% (25–85%) and 5% (1–45%) of the PSPT, respectively.

In liver cancer, the near-maximum doses to the skin were decreased to an average of 84% (72–95%) of the PSPT doses by the IMPT with the same beam angles. The D_{20} values of normal liver tissue after the removal of the GTV averaged 93% (78–100%) of the PSPT.

In prostate cancer, the near-maximum doses to the skin were varied using the IMPT into an average of 99% (84–111%) of the PSPT doses by the IMPT with the same beam angles. The D_{20} values of the rectum and bladder decreased to averages of 84% (77–88%) and 68% (32–98%) of the PSPT, respectively.

Broader beam angles tended to be effective for the optimization of the IMPT. The selection of the beam angles was significant, especially for nasal cavity cancer, because the IMPT had more choices of beam angle and the DVH for the OARs was sensitive to the beam angles as compared to other tumor sites. Meanwhile, in the liver and prostate cases, a change of about 10 degrees in the beam angle had little effect on the DVHs.

DISCUSSION

Target dose homogeneity

The IMPT could concentrate the dose on the PTV better than the PSPT, while the PTV dose homogeneity of the PTV tended to be worse. The degradation of the PTV dose homogeneity was caused by hotspots near the boundary of the PTV, which were created to enhance the dose contrast between the PTV and OARs, as shown in Fig. 4. The optimization of the IMPT prioritized the dose limitation of OARs above the PTV dose homogeneity. The better dose homogeneity of the PSPT was attributed to the use of the static ridge filers designed to administer a constant dose in the SOBP region and the placement of beam collimator close to the patient body surface.

Clinical advantage of the IMPT

The dose distribution and the DVHs were compared between the IMPT and PSPT in the treatment plans for typical cases of nasal cavity, lung, liver and prostate cancers. This study indicated that the DVHs of the OARs were improved by the use of IMPT for dose concentration to the PTV in nasal cavity, lung and prostate cancers, while they

were not significantly improved in liver cancer. The near-maximum doses to the skin were decreased by the use of IMPT in the nasal cavity, lung and liver cancers, while they were not greatly decreased in prostate cancer.

In the nasal cavity, the doses to the chiasm and optic nerves were significantly decreased by the use of IMPT. Therefore, the provability of visual disturbance was expected to be suppressed by the use of IMPT with optimization of beam angles. The maximum doses to the skin and OARs would be further decreased by outspreading and increasing the beam angles, although the irradiated volume would increase and might cause late side effects and radiation carcinogenesis. Outspreading and increasing the beam angles was difficult in PSPT because some intervening OARs could not be avoided while irradiating the PTV. On the other hand, with IMPT, intensity modulation made it possible to irradiate the PTV while administering a minimum dose to OARs in the radiation field. Improving the beam angles in IMPT was especially effective in treating nasal cavity cancer because the required beam ranges were shorter than about 17 cm from any direction, and most OARs were near the PTV.

In lung and liver cancer, the dose to the skin was decreased greatly by the use of IMPT. The DVHs of the normal lung and liver tissue showed little change since the lung and liver have large volumes as compared with the irradiated volumes. IMPT might be expected to avoid the fracturing of costal bones near the PTV in lung and liver cancer[22,23] by decreasing the dose to the costal bones along with the dose to the skin.

In prostate cancers, the near-maximum doses to the skin were not decreased, and so the use of IMPT would not reduce the probability of inflammation. However, the doses to the rectum and bladder were obviously decreased by IMPT, so the probabilities of rectal bleeding and irradiation cystitis would be expected to decrease.

The attempt to improve the beam angles used in IMPT from those in PSPT had little effect on the reduction of the dose to the OARs in lung, liver and prostate cancers. This might indicate that the optimal beam angles of the IMPT corresponded with those of the PSPT.

Respiratory displacement

It is well known that IMPT has a low tolerance for range uncertainty, setup error and the moving of body parts near the PTV. Many authors have advanced IMPT optimization algorithms that are robust against range uncertainty, setup error and/or the moving of the PTV.[24,25] In this study, we did not consider these problems so as to take notice of the geometrical advantages of the IMPT. The respiration-induced displacements of the lung and liver are generally larger than those of the nasal cavity and the prostate. For example, the amplitude of three-dimensional prostate movement was reported to be 0.1–2.7 mm in the supine position.[26] Meanwhile, the intrafractional lung tumor motion was reported to be 21.8 mm at a maximum for the GTV center of mass in the inferior direction in a respiratory-ungated case.[27] The tracks of respiration-induced liver tumor motion were reported to range from 3 to 50 mm.[28] Therefore, the dose distributions and DVHs calculated for liver and lung cancers will be complicated in a practical sense. Nasal cavity and prostate cancers will be good candidates for IMPT not only because of the geometrical advantage but also because they exhibit limited respiratory displacement.

ACKNOWLEDGMENTS

We would like to thank Takeshi Isui (ELEKTA) for his skillful support of the XiO software to plan the spot scanning for proton therapy. We also thank all members of the Proton Therapy Division at Shizuoka Cancer Center for their help. This study was performed as part of the cooperative research of the Shizuoka Cancer Center Research Institute and Mitsubishi Electric Corporation.

REFERENCES

1. Wilson R-R (1946) Radiological use of fast protons. Radiology **47**: 487–491.
2. ICRU (2007) Prescribing, Recording, and Reporting Proton-Beam Therapy. International Commission on Radiation Units and Measurements Report 78. Bethesda, MD.
3. Koehler A-M, Schneider R-J and Sisterson JM (1975) Range modulators for protons and heavy ions. Med Phys **131**: 437–440.
4. Koehler A-M, Schneider R-J and Sisterson J-M (1977) Flattening of proton dose distributions for large fields. Nucl Instrum Methods 4: 297–301.
5. Kanai T, *et al* (1980) Spot scanning system for radiotherapy. Med Phys 7: 365–369.
6. Furukawa T, *et al* (2010) Performance of the NIRS fast scanning system for heavy-ion radiotherapy. Med Phys **37**: 5672–5682.
7. Athar B-S and Paganetti H (2011) Comparison of second cancer risk due to out-of-field doses from 6-MV IMRT and proton therapy based on 6 pediatric patient treatment plans. Radiotherapy and Oncology **98**: 87–92.
8. Pedroni E, *et al* (1995) The 200-MeV proton therapy project at the Paul Scherrer Institute: conceptual design and practical realization. Med Phys **22**: 37–53.
9. Lomax A-J, *et al* (2001) Intensity modulated proton therapy: a clinical example. Med Phys **28**: 317–324.
10. Lomax A-J, *et al* (2004) Treatment planning and verification of proton therapy using spot scanning: Initial experiences. Med Phys **31**: 3150–3157.
11. Cozzi L, *et al* (2001) A treatment planning comparison of 3D conformal therapy, intensity modulated photon therapy and proton therapy for treatment of advanced head and neck tumours. Radiotherapy and Oncology **61**: 287–297.
12. Zhang X, *et al* (2010) Intensity-modulated proton therapy reduces the dose to normal tissue compared with intensity-modulated radiation therapy or passive scattering proton ther-

apy and enables individualized radical radiotherapy for extensive stage IIIB non-small-cell lung cancer: a virtual clinical study. Int J Radiat Oncol Biol Phys **77**: 357–366.
13. Murayama S, *et al* (2005) Initial clinical experience of proton therapy at Shizuoka Cancer Center, Nippon. Igaku Hoshasen Gakkai Zasshi **65**: 424–431.
14. Akagi T, *et al* (2003) Ridge filter design for proton therapy at Hyogo ion beam medical center. Phys Med Biol **48**: N301–N312.
15. Hong L, *et al* (1996) A pencil beam algorithm for proton dose calculations. Phys Med Biol **41**: 1305–1330.
16. Kanematsu N, *et al* (1998) A proton dose calculation code for treatment planning based on the pencil beam algorithm. Japan J Med Phys **18**: 88–103.
17. Russell K-R, *et al* (2000) Implementation of pencil kernel and depth penetration algorithms for treatment planning of proton beams. Phys Med Biol **45**: 9–27.
18. Kanematsu N, *et al* (2003) A CT calibration method based on the polybinary tissue model for radiotherapy treatment planning. Phys Med Biol **48**: 1053–1064.
19. Gottschalk B, Platais R and Paganetti H (1999) Nuclear interactions of 160 MeV protons stopping in copper: a test of Monte Carlo nuclear models. Med Phys **26**: 2597–2601.
20. Kimstrand P, *et al* (2007) A beam source model for scanned proton beams. Phys Med Biol **47**: 747–764.
21. Emami B, *et al* (1991) Tolerance of normal tissue to therapeutic irradiation. Int J Radiat Oncol Biol Phys **21**: 109–122.
22. Hashimoto T, *et al* (2006) Repeated proton beam therapy for hepatocellular carcinoma. Int J Radiat Oncol Biol Phys **65**: 196–202.
23. Andolino D-L, *et al* (2011) Chest wall toxicity after stereotactic body radiotherapy for malignant lesions of the lung and liver. Int J Radiat Oncol Biol Phys **80**: 692–697.
24. Unkelbach J, *et al* (2009) Reducing the sensitivity of IMPT treatment plans to setup errors and range uncertainties via probabilistic treatment planning. Med Phys **36**: 149–163.
25. Inaniwa T, *et al* (2011) Optimization algorithm for overlapping-field plans of scanned ion beam therapy with reduced sensitivity to range and setup uncertainties. Phys Med Biol **56**: 1653–1669.
26. Kitamura K, *et al* (2002) Three-dimensional intrafractional movement of prostate measured during real-time tumor-tracking radiotherapy in supine and prone treatment positions. Int J Radiat Oncol Biol Phys **53**: 1117–1123.
27. Dobashi S, *et al* (2011) Intrafractional respiratory motion for charged particle lung therapy with immobilization assessed by four-dimensional computed tomography. J Radiat Res **52**: 96–102.
28. Fuji H, *et al* (2009) Residual motion and duty time in respiratory gating radiotherapy using individualized or population-based windows. Int J Radiat Oncol Biol Phys **75**: 564–570.

Received on July 30, 2011
Revision received on September 27, 2011
Accepted on October 12, 2011
J-STAGE Advance Publication Date: December 1, 2011